ACS Photonics

pubs.acs.org/journal/apchd5

Letter

Multiple Scattering and Random Quasi-Phase-Matching in Disordered Assemblies of $LiNbO_3$ Nanocubes

Andrea Morandi,* Romolo Savo, Jolanda Simone Müller, Simeon Reichen, and Rachel Grange

Cite This: *ACS Photonics* 2022, 9, 1882−1888

Read Online

ACCESS | Metrics & More | Article Recommendations | Supporting Information

ABSTRACT: Nonlinear disordered photonic media (NDPM), composed of a random configuration of noncentrosymmetric crystals, offer a versatile platform to tailor nonlinear optical effects. The second-harmonic generation (SHG) and its random quasi-phase-matching (RQPM) in the multiple scattering regime are still poorly explored. In this work, we bottom-up assemble NDPM in two different geometries by using $LiNbO_3$ nanocubes as building blocks and investigate both the multiple scattering and the nonlinear properties. We produce disordered slabs with a continuously variable thickness and microspheres with different diameters, which display a remarkable strong light scattering, evidenced by a subwavelength transport mean free path (l^*). We first provide explicit evidence that the SHG power scales linearly with both the thickness of the slab and the volume of the microspheres. These observations generalize the characteristic linear scaling of RQPM power with the volume to the multiple scattering regime and to different sample geometries. Our structures represent a promising platform to investigate the interplay between disorder and optical nonlinear effects.

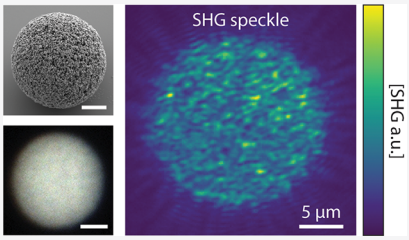

KEYWORDS: *Second-harmonic generation, bottom-up fabrication, transport mean free path, nonlinear optics*

INTRODUCTION

The study of disordered photonic media, in which the light is multiply scattered, is an active field in optics.[1,2] The interest ranges from fundamental transport properties such as Anderson localization,[3] the mean path length invariance,[4] and the anomalous diffusion of light,[5] to applications for laser sources[6] and in biomedical imaging.[7−9] Recently, an increasing interest has been dedicated to coherent nonlinear light generation in disordered photonic media, in particular to the second-harmonic generation (SHG).[10,11] One advantage is that photonic disorder relaxes the stringent phase-matching conditions of high-quality crystals, enabling a broadband harmonic generation independently from the pump polarization.

SHG in disordered media has been extensively studied in transparent polycrystals within the random quasi-phase-matching (RQPM) framework.[12,13] This considers a disordered distribution of non-scattering $\chi^{(2)}$ domains that generates nonlinear waves with random amplitude and phase, under the excitation of a pump beam. The interference of the SHG from the many random sources leads to a global SHG, whose power scales linearly with the sample thickness. This linear scaling, whose properties have been investigated in recent numerical studies,[14−16] is a fingerprint of RQPM,[12] since it is in contrast to the quadratic scaling of both phase-matched and quasi-phase-matched crystals.[17]

Differently to the typical RQPM scenario, nonlinear disordered photonic media (NDPM) can have noncentrosymmetric domains that are also scattering sites. Recently, several studies have investigated the SHG generated from a NDPM in the multiple scattering regime focusing on properties, such as the intensity distribution,[18] the polarization dependency,[19] and the nonlinear speckle pattern.[20] Nonetheless, investigating the robustness of the RQPM scaling in the multiple scattering regime presents several experimental challenges. The first difficulty lies in the material fabrication, which requires combining multiple scattering and second-order nonlinearity in a single medium. The second difficulty is the accurate characterization of both the scattering and the nonlinear properties.

Kurtz and Perry first reported the SHG from a scattering powder obtained by grinding the bulk materials in smaller grains of about 10 μm.[21] They only mentioned the linear scaling of the SHG with the powder thickness, without displaying the results and with no characterization of the scattering strength of the powder. Several experimental studies on SHG in NDPM were carried out on electrochemically etched GaP and GaAs slabs, which show a large second-order nonlinearity and remarkably strong scattering properties thanks to their porous (network-like) structure.[22−24] Using a slab of porous GaP, Faez et al.[25] studied the SHG in a carefully

Received: February 5, 2022
Published: June 2, 2022

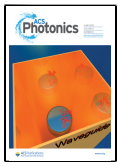

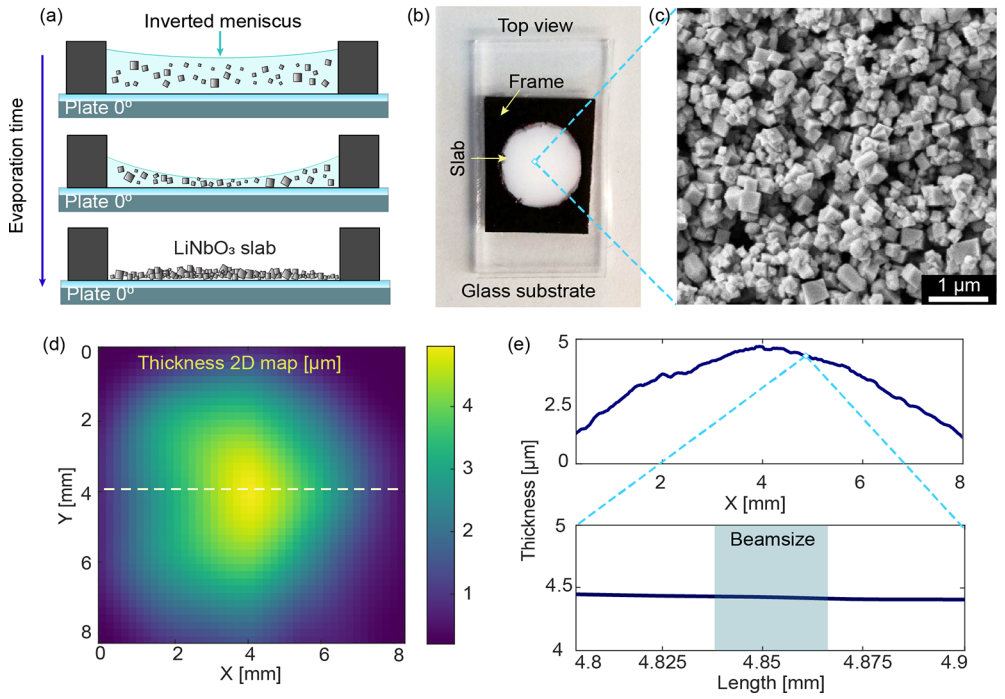

Figure 1. Fabrication and thickness characterization of disordered $LiNbO_3$ slabs. (a) Schematic of the inverted meniscus technique to avoid the coffee ring effect. The contact angle between the liquid and the frame ensures a uniform deposition in the center of the sample. (b) Top view of a typical sample. Prior to the deposition, the substrate was cleaned with acetone and ethanol, followed by 10 min of plasma cleaning. The white circle is the slab and the black frame around it is the tape. The slab is unsealed from the top. (c) SEM image of the slab surface composed of nanocubes of $LiNbO_3$. (d) 2D map of the thickness of the slab measured by profilometry technique. (e) Measured thickness along the white dashed line reported in (d) with a close-up on a smaller region of 0.1 mm. The sample can be considered flat on the length scale of the beam diameter (30 μm).

characterized multiple scattering regime. They also observed the linear increase of the emitted SHG power with the sample thickness, but did not display the data. Indeed, to measure the SHG scaling, they used multiple samples with increasing thicknesses, which were etched independently, potentially generating different internal structures. This lack of control on the size distribution of the crystalline nanodomains, may introduce systematic differences in both the SHG and the scattering properties of the samples. As a result, there is no explicit demonstration of the RQPM scaling for the SHG in nonlinear disordered photonic materials, although the effect has been clearly predicted by models combining RQPM and the light diffusion hypothesis.[25,26]

In this work, we fabricate nonlinear disordered photonic media by bottom-up assembly of lithium niobate ($LiNbO_3$) nanocubes into slabs of variable thicknesses as well as into regular microspheres of different diameters. The size distribution is known thanks to the a priori characterization on the crystalline nanocubes, as well as to the absence of an etching phase. We provide explicit evidence of RQPM in the multiple scattering regime by showing the linear scaling of the transmitted SHG power with the slab thickness as well as with the volume of the microspheres. Both the slab and the microspheres display a remarkably strong scattering in the red part of the visible spectrum and hint to an even stronger scattering regime at shorter wavelengths (blue to the ultraviolet), for which signs of Anderson localization are expected.[3,27] Thanks to their peculiar features and to the convenient bottom-up fabrication method, the presented assemblies are a suitable platform to investigate the interplay between linear and nonlinear optical phenomena in the multiple scattering regime.

RESULTS AND DISCUSSION

We assembled the slabs and the microspheres starting from crystalline $LiNbO_3$ nanocubes that were produced via solvothermal synthesis, following the procedure detailed in the work by Timpu et al.[28] This chemical synthesis allows for a precise control of the size distribution of the produced nanoparticles. Additionally, it prevents the creation of defects and strain, common when grinding wafers to powders, which can cause undesired sub-band gap absorption.[29] The nanocubes have sizes ranging from 100 to 400 nm, a refractive index of $n \approx 2.3$ and negligible absorption at visible wavelengths.[30,31] Despite the nanometer size, they maintain the noncentrosymmetric hexagonal $R3c$ crystal structure of bulk $LiNbO_3$ that enables SHG. Moreover, experiments on single nanocubes have evidenced geometry-dependent optical properties, such as a Mie-resonant scattering cross-section in the blue and near UV and the consequent enhancement of the SHG efficiency.[28]

NANOCUBES ASSEMBLED IN SLABS

We assembled the nanocubes into slabs by drop deposition and solvent evaporation. An aqueous suspension (2 wt %) of the $LiNbO_3$ nanocubes was mixed with 30% poly(vinyl alcohol) and deposited over a glass substrate framed with hydrophilic tape, as depicted in Figure 1a. The sample was placed onto a horizontal substrate holder within an isolating box filled with ice water to keep the sample at 0 °C. After 36 h, the nanocubes were deposited and the water had evaporated. In a droplet drying on a flat hydrophilic surface, a faster evaporation occurs at the edges of the droplet, and this generates an outward flow responsible for the accumulation of the solute at the borders, a phenomenon known as the coffee-ring effect.[32,33] We prevented this effect by adding the frame,

https://doi.org/10.1021/acsphotonics.2c00210
ACS Photonics 2022, 9, 1882−1888

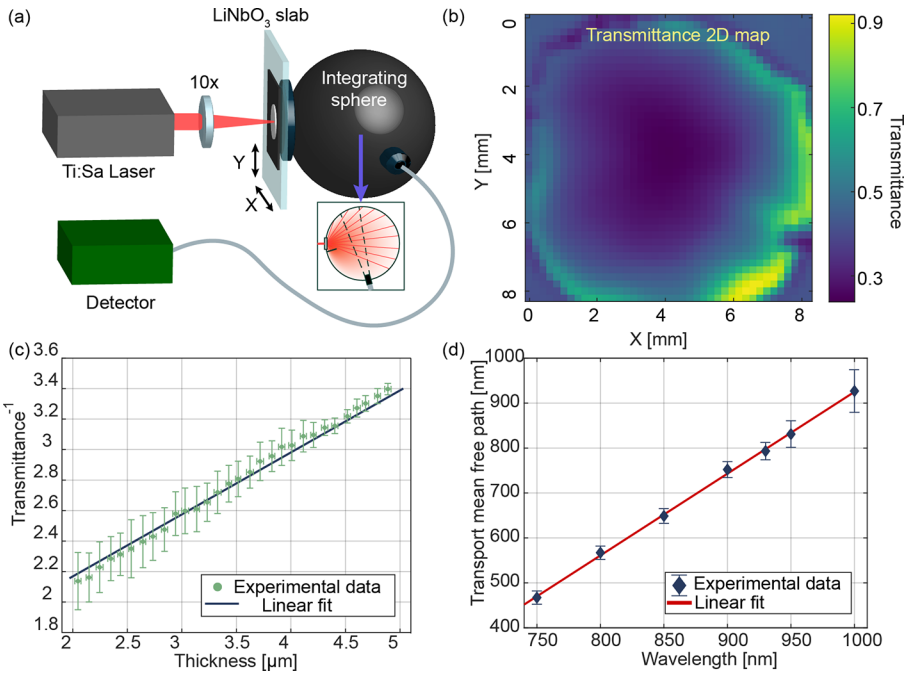

Figure 2. Characterization of the scattering properties of the slabs. (a) Schematic of the setup with the sample placed on motorized stages to access the 1 cm^2 surface and with an integrating sphere to collect the transmitted light. The inset depicts the working principle of the integrating sphere. (b) Measured 2D map of the transmittance measured at 930 nm of pump. (c) Reciprocal total transmittance over the thickness with the linear fit, the error bars represent the standard deviation of all the data collected at the same thickness. (d) Transport mean free path for different wavelengths between 750 and 1000 nm; additional plots in Figure S3.

which ensured that the meniscus of the suspension stayed concave during the evaporation of the water. This inverted meniscus technique made the suspension evaporate first in the center of the droplet such that the resulting internal capillary flow carried most of the nanocubes toward the center of the droplet where they were deposited. Under visible light illumination, the slabs have the white appearance that is typical of multiple scattering media, Figure 1b. The scanning electron microscopy (SEM) image reported in Figure 1c reveals that the nanocubes are uniformly packed across the lateral size of the slab with a volumetric filling fraction of 55 ± 5%, as measured by image analysis (see Supporting Information, Figure S1). Figure 1d shows a map of the slab thickness over the entire sample area and Figure 1e a cross section of this map. The slab thickness has a maximum at the center of the sample and decreases smoothly along the radial direction. In this condition, the sample is effectively flat on a length scale much larger than the slab thickness and multiple thicknesses can be readily obtained by translating the sample with respect to the laser beam.

A quantification of the scattering strength of the slab was carried out by measuring the scaling of the total transmission with the thickness, which allows one to retrieve the transport mean free path l^*.[34] The experimental setup used for this procedure is depicted in Figure 2a. The light from a Ti:Sa laser is focused onto the sample at the entrance port of an integrating sphere. The transmitted light is collected within the sphere and a part of it is guided to a power-meter through a fiber. A 2D map of its transmittance at 930 nm wavelength is shown in Figure 2b. The measurement was obtained by moving the sample in the plane orthogonal to the pump beam with a 200 μm pitch between measurement points. This choice guarantees that each transmission value refers to an independent configuration of the sample disorder. Through point-by-point matching of the transmittance map (Figure 2b) with the thickness map (Figure 1a), we derived the scaling relation reported in Figure 2c between the inverse of the total transmission and the slab thickness. Modeling of the data with the photonic Ohm's law reported in eq 1[35] allows us to retrieve the transport mean free path l^*

$$T(\lambda) = \frac{l^*(\lambda) + z_0(\lambda)}{L + 2z_0(\lambda)} \tag{1}$$

Here, L is the thickness of the sample, $z_0(\lambda) = \frac{2}{3} l^*(\lambda) \frac{1 + R_i}{1 - R_i}$ is the extrapolation length, and R_i is the internal reflectivity calculated with Fresnel laws by using the effective refractive index of the slab (Figure S2). The basic assumption of eq 1 is the diffusive propagation of light within the slab. To fit the experimental data, eq 1 can be recast in the following eq 2:

$$\frac{1}{T(\lambda)} = \frac{1}{l^*(\lambda) + z_0(\lambda)} L + \frac{2z_0(\lambda)}{l^*(\lambda) + z_0(\lambda)} \tag{2}$$

in which l^* is the only free parameter. The characterization of the scattering strength was performed at several wavelengths between 750 and 1000 nm. The linear fit obtained by applying the model to the data measured at 930 nm is reported in Figure 2c. The obtained values of l^* are displayed in Figure 2d and reported in Table 1. For all considered cases, l^* has a subwavelength size, which is smaller than the slab thickness (5 μm), providing evidence of the strong light scattering within the slab and of the multiple scattering regime (see Table 1). The obtained values of l^* appear particularly interesting looking at the corresponding inverse scattering efficiency $kl^* = 2\pi l^*/\lambda$. As this parameter gets closer to 1, the diffusive regime reaches its limit of validity and signs of Anderson localization of light can emerge.[3,27] Our sample shows a

https://doi.org/10.1021/acsphotonics.2c00210
ACS Photonics 2022, 9, 1882−1888

Table 1. Transport Mean Free Path and Inverse Scattering Coefficient at Different Pump Wavelengths

wavelength (nm)	l^* (nm)	$k \cdot l^*$
750	476 ± 6	3.9 ± 0.1
800	567 ± 7	4.4 ± 0.1
850	649 ± 8	4.8 ± 0.1
900	752 ± 12	5.3 ± 0.1
930	788 ± 14	5.4 ± 0.1
950	831 ± 22	5.5 ± 0.2
1000	927 ± 34	5.8 ± 0.2

$kl^* = 3.9$ at 750 nm, which is close to the smallest value reported for visible light of 2.6.[22] Moreover, the observed linear decrease of kl^* with the wavelength, reported in Figure 2d, suggests that a kl^* closer to 1 (i.e., stronger scattering) could be reached at wavelengths shorter than 750 nm. This possibility of a continuous decrease of kl^* is also supported by the resonant scattering cross-section and wide transparency window of the individual nanocubes in the blue spectral region.[28]

We performed the nonlinear characterization of the disordered slabs by collecting the transmitted SHG with a microscope objective (Zeiss 100×), after filtering out the fundamental pump wavelength. As for the transmittance, a 2D map of the SHG was obtained by laterally moving the sample with respect to the laser beam. The result is shown in Figure 3a. Similarly to the linear measurements, we established a one to one correspondence between the thickness and the SHG maps, obtaining the SHG power scaling with the slab thickness reported in Figure 3b. Fitting this data with the power law $y = \beta x^{\alpha}$ returns an exponent of $\alpha = 0.98 \pm 0.03$. This observation agrees with the theoretical prediction derived for the SHG in a multiple scattering medium,[26] which predicts that both the forward- and the backward-emitted SHG power grow linearly with the slab thickness.[36] The linearity of the scaling relation provides evidence of RQPM in the presence of multiple scattering of the pump and of the SHG light. This linear scaling is a key result of this study, which has not been reported explicitly in previous works. Interestingly, our measurement shows a deviation from the predicted linear trend at larger thicknesses (above 4 μm). A possible explanation might be found in the hypothesis of the considered model, which assumes a diffusive regime for the multiple scattered light, that is, a slab thickness much larger than l^*. The thicknesses of our slab spans from 2 to 10 transport mean free paths, hence, we might be observing a transition between two different linear scalings of the SHG due to a redistribution between the forward- and backward-emitted SHG.[25] Up to which extent the SHG power scaling with the volume depends on the geometry of the sample is an open question. Indeed, the compensation mechanism leading to the linear scaling of the SHG intensity with the slab thickness, or equivalently of the SHG power with the volume, is in principle geometry-dependent since the specific light distribution depends on the sample geometry. We tackled this question considering samples with a nonslab geometry, in particular, by fabricating disordered microspheres that multiply scattered light and by investigating the scaling of the SHG with the volume.

NANOCUBES ASSEMBLED IN MICROSPHERES

We fabricated the disordered microspheres by using the same $LiNbO_3$ nanocubes that we used for the slabs. We used an emulsion-templated assembly technique,[37,38] consisting in mixing 10 μL of aqueous dispersion of the nanocubes (2 wt %) with 1 mL of surfactant-loaded (10 wt % SPAN 80) hexadecane, followed by an emulsification process obtained though mechanical shaking. This generates a polydispersed distribution of water-in-oil droplets filled with the nanocubes, which are collected and then deposited on a glass substrate with a pipet (Figures S4 and S5). The water in the droplets diffuses into the oil, shrinking the size of the droplets and forcing the nanocubes to assemble into microspheres, as depicted in Figure 4a. During this process, the Brownian motion of the nanocubes in the droplets ensures that each nanocube is positioned and oriented randomly within the microsphere. The obtained microspheres have diameters ranging from 2 to 40 μm.

An optical image of a microsphere with 35 μm diameter is shown in Figure 4b. Its white appearance, similar to the slab sample, is a solid indication of multiple light scattering. In these spherical assemblies the transport mean free path l^* cannot be directly measured with the technique employed

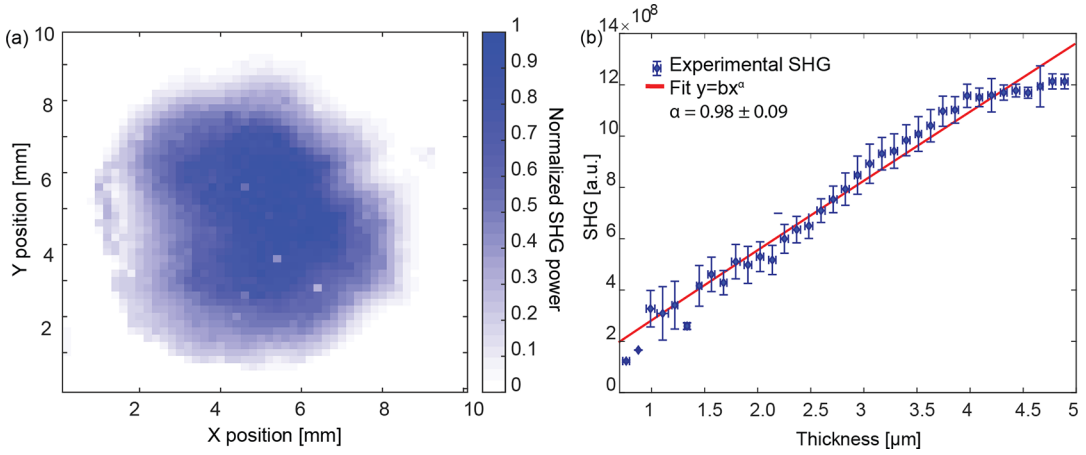

Figure 3. SHG measurements from a $LiNbO_3$ slab. (a) 2D map of the SHG for the pump at 930 nm of pump. As expected the SHG intensity is maximal for the maximum thickness. (b) SHG power at different sample thicknesses. Every point is an average over many measurements with comparable thickness, and the error bars are given by the standard deviation of these measurements. In the thickest part of the sample, we observe a reduction of the slope likely caused by the increase of the backscattered SHG in comparison to the forward transmitted one.

https://doi.org/10.1021/acsphotonics.2c00210
ACS Photonics 2022, 9, 1882−1888

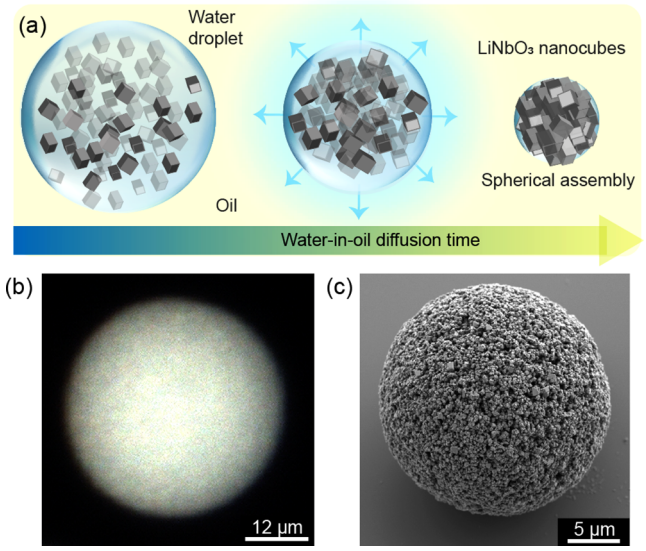

Figure 4. Fabrication of the $LiNbO_3$ microspheres. (a) Principle of the emulsion-templated assembly of the $LiNbO_3$ spheres. (b) Dark-field microscopy image of an assembled microsphere obtained with a 50× apochromat objective. The white appearance suggests that the light undergoes multiple scattering in the microspheres. (c) Scanning electron micrograph image of an assembled microsphere, which was also used to precisely measure the volume the microspheres. A few larger cubes (600 nm) can be seen on the surface, with a negligible impact on the properties of the assembly due to their rarity.

before, since the photonic Ohm's law strictly applies to the slab geometry.[35] Nonetheless, it is possible to estimate the l^* of the microspheres through the analysis of different SEM images, like the one displayed in Figure 4c. This returns a volumetric filling fraction $ff = 52 \pm 4\%$ (Figure S1), which is slightly smaller than that of the slabs $ff = 55 \pm 5$. From this filling fraction we can estimate that the transport mean free path of our microspheres should be equal to or shorter than those measured for the slab samples (Table 1). This estimation follows from the fact that the transport mean free path of a disordered assembly is minimal (i.e., strongest scattering) around a filling fraction of 30% and it increases for denser structures,[39] like our microspheres.

The nonlinear optical properties of the spheres were characterized by using the setup depicted in Figure 5a,b. We illuminated the microspheres with the same laser pulses that were used for the slab experiment at $\lambda = 930$ nm and collected the SHG in transmission with a microscope objective (50× Zeiss apochromat). The spectral measurement as well as the quadratic power-scaling of the nonlinear signal, shown in Figures S7 and S8, confirm that we are detecting SHG from the sample. The SHG emitted by 25 microspheres with diameters between 1 and 15 μm is shown in Figure 5c. Power-law fitting with the function $y = \alpha x^{\beta}$ returns a best-fit exponent of $\beta = 2.76 \pm 0.34$, which corresponds to a linear scaling of the SHG power with the volume of the assembly (i.e., with the number of nanocubes), as shown in the inset of Figure 5c. In the case of a sphere, in which conventional diffusive equations are challenging to solve due to nontrivial boundary conditions, we retrieve a linear trend of the SHG power versus the volume. This observation demonstrates that the compensation mechanism discussed before for the slab case, that is, that the laterally growing illuminated volume and the continuously attenuated pump power compensate to return the typical scaling of RQPM for transparent media,[26] applies to a larger class of sample geometry. The bigger microspheres (above 8 μm) slightly deviate from the linear trend, which can be explained with a partial redistribution from transmitted to backscattered SHG, similarly to the behavior in the slabs shown in Figure 3b. An alternative explanation for the observed deviation could be that the diameter of the microspheres gets comparable to the size of the Gaussian profile of the pump beam (fwhm 18 μm) and that, therefore, the bigger microspheres of the data set are illuminated with less average intensity than the smaller ones.

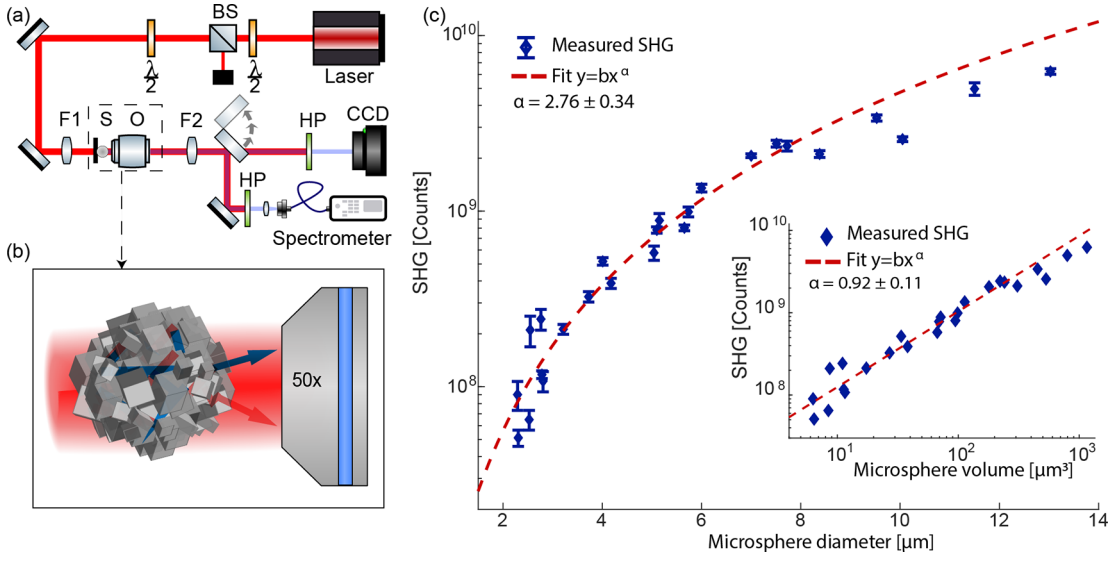

Figure 5. Nonlinear optical characterization of the microspheres. (a) Schematic of the setup used to measure the SHG. (b) Sketch of the fundamental beam propagating in the assembly together with the second harmonic generated light. (c) SHG scaling with the microspheres diameter and data fit with a power law function, proving the linear scaling with the volume, signature of the RQPM regime. Inset: SHG reported as a function of the microspheres volume, explicitly showing the linear scaling with volume over more than 2 orders of magnitude.

https://doi.org/10.1021/acsphotonics.2c00210
ACS Photonics 2022, 9, 1882−1888

CONCLUSIONS

We used $LiNbO_3$ nanocubes with two different bottom-up assembly techniques to fabricate nonlinear disordered photonic media with both slab and spherical geometry. We investigated RQPM for the SHG in the multiple scattering regime by experimentally looking at the scaling of the SHG with sample size for two geometries of the multiple scattering medium. The presented fabrication methods enable varying the sample size while keeping both the scattering strength and the nonlinear optical properties stable. Characterization of the scattering strength returned a minimal value of l^* of 476 ± 6 at 750 nm wavelength, corresponding to an inverse scattering coefficient of 3.9 ± 0.1. This value and the observed decreasing trend with the wavelength makes our samples a promising platform to study the Anderson localization of the SHG in three-dimensional multiple scattering media with second-order nonlinearity, which is an unusual physical scenario.[18] The observed linear scaling of the SHG power with the slab thickness provides the first explicit evidence of RQPM in the multiple scattering regime. An equivalent linear scaling of the SHG power with the volume is observed for the disordered microspheres, showing that the RQPM scaling is independent of the geometry of the multiple scattering sample. A linear scaling of the SHG power with the volume of the microspheres was recently reported in the regime where the microspheres are transparent and resonant at the pump wavelength.[13] This common behavior suggests the presence of a fundamental property that regulates the energy distribution of both the pump and the SHG, presumably related to the property of the mean path length invariance.[4] This aspect represents an interesting direction for future investigation. Another open question is what happens to the slope of the SHG scaling with the volume of the sample in assemblies built with nearly monodisperse nanocubes as their size influences both the scattering strength and the efficiency of the generation. Thanks to their complementary properties, we propose $LiNbO_3$ bottom-up assembled NDPM as a platform to study the interplay of coherent nonlinear generation and multiple scattering of light.[11,40]

ASSOCIATED CONTENT

Supporting Information

The Supporting Information contains: The Supporting Information is available free of charge at https://pubs.acs.org/doi/10.1021/acsphotonics.2c00210.

> The study of the filling fraction from image analysis; The effective refractive index calculation to estimate the extrapolation length z_0; The measurements of the transport mean free path at wavelengths 750−1000 nm; Details on the drying emulsions fabrication process; The spectrum and power dependence of the SHG from the microspheres (PDF)

AUTHOR INFORMATION

Corresponding Author

Andrea Morandi − *ETH Zurich, Institute for Quantum Electronics, Department of Physics, Optical Nanomaterial Group, 8093 Zurich, Switzerland;* orcid.org/0000-0001-8199-1536; Email: morandia@phys.ethz.ch

Authors

Romolo Savo − *ETH Zurich, Institute for Quantum Electronics, Department of Physics, Optical Nanomaterial Group, 8093 Zurich, Switzerland*

Jolanda Simone Müller − *ETH Zurich, Institute for Quantum Electronics, Department of Physics, Optical Nanomaterial Group, 8093 Zurich, Switzerland*

Simeon Reichen − *ETH Zurich, Institute for Quantum Electronics, Department of Physics, Optical Nanomaterial Group, 8093 Zurich, Switzerland*

Rachel Grange − *ETH Zurich, Institute for Quantum Electronics, Department of Physics, Optical Nanomaterial Group, 8093 Zurich, Switzerland;* orcid.org/0000-0001-7469-9756

Complete contact information is available at: https://pubs.acs.org/10.1021/acsphotonics.2c00210

Funding

The project has received funding from the European Union's Horizon 2020 research and innovation program under the Marie Skłodowska-Curie Grant Agreement No. 800487 (SECOONDO) and from the European Research Council under Grant Agreement No. 714837 (Chi2-nano-oxides). We thank the Swiss National Science Foundation (SNF) Grant 150609.

Notes

The authors declare no competing financial interest.

ACKNOWLEDGMENTS

We acknowledge Maria Teresa Buscaglia and Vincenzo Buscaglia from the Institute of Condensed Matter Chemistry and Technologies for Energy (National Research Council, via De Marini 6, 16149 Genoa, Italy) for the synthesis of the nanocubes. We acknowledge support from the FIRST—Center for Micro and Nanoscience of ETHZ and from the Scientific Center of Optical and Electron Microscopy (ScopeM) of ETHZ.

REFERENCES

(1) Wiersma, D. S. Disordered photonics. *Nat. Photonics* **2013**, *7*, 188−196.

(2) Rotter, S.; Gigan, S. Light fields in complex media: Mesoscopic scattering meets wave control. *Rev. Mod. Phys.* **2017**, *89*, 1.

(3) Wiersma, D. S.; Bartolini, P.; Lagendijk, A.; Righini, R. Localization of light in a disordered medium. *Nature* **1997**, *390*, 671−673.

(4) Savo, R.; Pierrat, R.; Najar, U.; Carminati, R.; Rotter, S.; Gigan, S. Mean path length invariance in multiple light scattering. *Science* **2017**, *358*, 765−768.

(5) Barthelemy, P.; Bertolotti, J.; Wiersma, D. S. A Lévy flight for light. *Nature* **2008**, *453*, 495−498.

(6) Wiersma, D. S. The physics and applications of random lasers. *Nat. Phys.* **2008**, *4*, 359−367.

(7) Campagnola, P. J.; Loew, L. M. Second-harmonic imaging microscopy for visualizing biomolecular arrays in cells, tissues and organisms. *Nat. Biotechnol.* **2003**, *21*, 1356−1360.

(8) Tilbury, K. B.; Campbell, K. R.; Eliceiri, K. W.; Salih, S. M.; Patankar, M.; Campagnola, P. J. Stromal alterations in ovarian cancers via wavelength dependent Second Harmonic Generation microscopy and optical scattering. *BMC Cancer* **2017**, *17* (17), 102.

(9) Moretti, C.; Gigan, S. Readout of fluorescence functional signals through highly scattering tissue. *Nat. Photonics* **2020**, *14*, 361−364.

(10) Fischer, R.; Saltiel, S. M.; Neshev, D. N.; Krolikowski, W.; Kivshar, Y. S. Broadband femtosecond frequency doubling in random media. *Appl. Phys. Lett.* **2006**, *89*, 191105.
(11) Qiao, Y.; Ye, F.; Zheng, Y.; Chen, X. Cavity-enhanced second-harmonic generation in strongly scattering nonlinear media. *Phys. Rev. A* **2019**, *99*, 43844.
(12) Baudrier-Raybaut, M.; Haïdar, R.; Kupecek, P.; Lemasson, P.; Rosencher, E. Random quasi-phase-matching in bulk polycrystalline isotropic nonlinear materials. *Nature* **2004**, *432*, 374−376.
(13) Savo, R.; Morandi, A.; Müller, J. S.; Kaufmann, F.; Timpu, F.; Reig Escalé, M.; Zanini, M.; Isa, L.; Grange, R. Broadband Mie driven random quasi-phase-matching. *Nat. Photonics* **2020**, *14*, 740−747.
(14) Chen, X.; Gaume, R. Non-stoichiometric grain-growth in ZnSe ceramics for χ (2) interaction. *Optical Materials Express* **2019**, *9*, 400.
(15) Kawamori, T.; Ru, Q.; Vodopyanov, K. L. Comprehensive Model for Randomly Phase-Matched Frequency Conversion in Zinc-Blende Polycrystals and Experimental Results for ZnSe. *Phys. Rev. Appl.* **2019**, *11*, 1.
(16) Müller, J. S.; Morandi, A.; Grange, R.; Savo, R. Modeling of Random Quasi-Phase-Matching in Birefringent Disordered Media. *Phys. Rev. Appl.* **2021**, *15*, 1.
(17) Nonlinear, R. W. *Nonlinear Opt.*; Elsevier, 2008.
(18) Skipetrov, S. E.; Sokolov, I. M. Intensity of Waves Inside a Strongly Disordered Medium. *Phys. Rev. Lett.* **2019**, *123*, 233903.
(19) Sánchez-Dena, O.; Behel, Z.; Salmon, E.; Benichou, E.; Reyes-Esqueda, J. A.; Brevet, P. F.; Jonin, C. Polarization-resolved second harmonic generation from LiNbO3 powders. *Opt. Mater.* **2020**, *107*, 110169.
(20) Samanta, R.; Mujumdar, S. Intensity-dependent speckle contrast of second harmonic light in a nonlinear disordered medium. *Appl. Opt.* **2020**, *59*, 11266.
(21) Kurtz, S. K.; Perry, T. T. 6F-9 A Powder Technique for the Evaluation of Nonlinear Optical Materials. *IEEE J. Quantum Electron.* **1968**, *4*, 333.
(22) Schuurmans, F. J.; Vanmaekelbergh, D.; Van De Lagemaat, J.; Lagendijk, A. Strongly photonic macroporous gallium phosphide networks. *Science* **1999**, *284*, 141−143.
(23) Mel'nikov, V. A.; Golovan, L. A.; Konorov, S. O.; Muzychenko, D. A.; Fedotov, A. B.; Zheltikov, A. M.; Timoshenko, V. Y.; Kashkarov, P. K. Second-harmonic generation in strongly scattering porous gallium phosphide. *Applied Physics B: Lasers and Optics* **2004**, *79*, 225−228.
(24) Tiginyanu, I. M.; Kravetsky, I. V.; Monecke, J.; Cordts, W.; Marowsky, G.; Hartnagel, H. L. Semiconductor sieves as nonlinear optical materials. *Appl. Phys. Lett.* **2000**, *77*, 2415−2417.
(25) Faez, S.; Johnson, P. M.; Mazurenko, D. A.; Lagendijk, A. Generation and Diffusion Inside Random Media. *Journal of the Optical Society of America B* **2009**, *26*, 235−243.
(26) Makeev, E. V.; Skipetrov, S. E. Second harmonic generation in suspensions of spherical particles. *Opt. Commun.* **2003**, *224*, 139−147.
(27) Sperling, T.; Schertel, L.; Ackermann, M.; Aubry, G. J.; Aegerter, C. M.; Maret, G. Can 3D light localization be reached in 'white paint'? *New J. Phys.* **2016**, *18*, 013039.
(28) Timpu, F.; Sendra, J.; Renaut, C.; Lang, L.; Timofeeva, M.; Buscaglia, M. T.; Buscaglia, V.; Grange, R. Lithium Niobate Nanocubes as Linear and Nonlinear Ultraviolet Mie Resonators. *ACS Photonics* **2019**, *6*, 545−552.
(29) Van Der Beek, T.; Barthelemy, P.; Johnson, P. M.; Wiersma, D. S.; Lagendijk, A. Light transport through disordered layers of dense gallium arsenide submicron particles. *Phys. Rev. B: Condensed Matter Mater. Phys.* **2012**, *85*, 1−11.
(30) Weis, R. S.; Gaylord, T. K. Lithium niobate: Summary of physical properties and crystal structure. *Applied Physics A Solids and Surfaces* **1985**, *37*, 191−203.
(31) Volk, T.; Wöhlecke, M. *Lithium Niobate: Defects, Photorefraction, and Ferroelectric Switching*, Springer Series in Materials Science; 2008; Vol. *115*; pp 1−249,
(32) Mampallil, D.; Eral, H. B. A review on suppression and utilization of the coffee-ring effect. *Adv. Colloid Interface Sci.* **2018**, *252*, 38−54.
(33) Li, Y. F.; Sheng, Y. J.; Tsao, H. K. Evaporation stains: Suppressing the coffee-ring effect by contact angle hysteresis. *Langmuir* **2013**, *29*, 7802−7811.
(34) Martelli, F.; Contini, D.; Taddeucci, A.; Zaccanti, G. Photon migration through a turbid slab described by a model based on diffusion approximation II Comparison with Monte Carlo results. *Appl. Opt.* **1997**, *36*, 4600.
(35) Sapienza, R.; García, P. D.; Bertolotti, J.; Martín, M. D.; Blanco, Á.; Viña, L.; López, C.; Wiersma, D. S. Observation of resonant behavior in the energy velocity of diffused light. *Phys. Rev. Lett.* **2007**, *99*, 233902.
(36) De Boer, J. F.; Lagendijk, A.; Sprik, R.; Feng, S. Transmission and reflection correlations of second harmonic waves in nonlinear random media. *Phys. Rev. Lett.* **1993**, *71*, 3947−3950.
(37) Kim, S. H.; Lee, S. Y.; Yi, G. R.; Pine, D. J.; Yang, S. M. Microwave-assisted self-organization of colloidal particles in confining aqueous droplets. *J. Am. Chem. Soc.* **2006**, *128*, 10897−10904.
(38) Vogel, N.; Utech, S.; England, G. T.; Shirman, T.; Phillips, K. R.; Koay, N.; Burgess, I. B.; Kolle, M.; Weitz, D. A.; Aizenberg, J. Color from hierarchy: Diverse optical properties of micron-sized spherical colloidal assemblies. *Proc. Natl. Acad. Sci. U.S.A.* **2015**, *112*, 10845−10850.
(39) Pattelli, L.; Egel, A.; Lemmer, U.; Wiersma, D. S. Role of packing density and spatial correlations in strongly scattering 3D systems. *Optica* **2018**, *5*, 1037.
(40) Qiao, Y.; Peng, Y.; Zheng, Y.; Ye, F.; Chen, X. Second-harmonic focusing by a nonlinear turbid medium via feedback-based wavefront shaping. *Optics letters* **2017**, *42*, 1895−1898.

https://doi.org/10.1021/acsphotonics.2c00210
ACS Photonics 2022, 9, 1882−1888